COMPUTATIONAL BEAM DYNAMICS REQUIREMENTS FOR FRIB*

P. N. Ostroumov[†], Y. Hao, T. Maruta, A. Plastun, T. Yoshimoto, T. Zhang, Q. Zhao
Facility for Rare Isotope Beams, Michigan State University, East Lansing, MI, USA

Abstract

The Facility for Rare Isotope Beams (FRIB) being built at Michigan State University moved to the commissioned stage in the summer of 2017. There were extensive beam dynamics simulations in the FRIB driver linac during the design stage. Recently, we have used TRACK and IM-PACT simulation codes to study dynamics of ion beam contaminants extracted from the ECR together with main ion beam. The contaminant ion species can produce significant uncontrolled losses after the stripping. These studies resulted in development of beam collimation system at relatively low energy of 17 MeV/u and room temperature bunchers instead of originally planned SC cavities. Commissioning of the Front End and the first 3 cryomodules enabled detailed beam dynamics studies experimentally which were accompanied with the simulations using above-mentioned beam dynamics codes and envelope code FLAME with optimizers. There are significant challenges in understanding of beam dynamics in the FRIB linac. The most computational challenges are in the following areas: (1) Simulation of the ion beam formation and extraction from the ECR; (2) Development of the virtual accelerator model available on-line both for optimization and multi-particle simulations. The virtual model should include realistic accelerator parameters including device misalignments; (3) Large scale simulations to support high-power ramp up of the linac with minimized beam losses; (4) Extension of the existing codes for large scale simulations to support tuning of fragment separators for selected isotopes.

INTRODUCTION

The Facility for Rare Isotope Beams (FRIB) currently being built at Michigan State University (MSU) is the next generation facility for rare isotope science. The FRIB includes a high-power driver accelerator, a target, and fragment separators. The FRIB driver linac will provide stable nuclei accelerated to 200 MeV/u for the heaviest uranium ions and higher energies for lighter ions with 400 kW power on the target [1]. FRIB features a continuous wave (CW) linac with a room-temperature 0.5 MeV/u front-end followed by a superconducting radiofrequency (SRF) linac consisting of 4 types of niobium cavities. The first SRF section includes quarter-wave resonators (QWR) with β_{OPT}=0.041 and β_{OPT}=0.085 which accelerate ion beams from 0.5 MeV/u to ~20 MeV/u at the charge stripper. The optimal beta is defined as relative velocity, β_{OPT}, where the maximum transit time factor T is achieved. The ion beams are further accelerated with the half-wave resonators

(HWR) of β_{OPT} =0.29 and β_{OPT} =0.53. Total 316 SRF cavities are used for acceleration to the design energy of 200 MeV/u for heaviest uranium ions. 400 kW accelerated ion beams will be delivered to the target which is followed by a large acceptance high resolution fragment separator. While many isotopes will be studied in the in-flight experiments, FRIB will use upgraded National Superconducting Cyclotron Laboratory (NSCL) facilities to prepare and re-accelerate stopped isotopes up to 12 MeV/u. Currently, the re-accelerator (ReA3), consisting of a radiofrequency quadrupole (RFQ) and a superconducting radio-frequency (SRF) linac provides 3 MeV/u rare isotope beams for experiments.

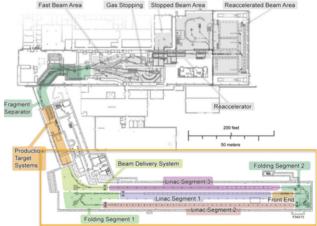The layout of the FRIB is shown in Fig. 1.

Figure 1: Layout of the FRIB driver accelerator, target, fragment separator, re-accelerator and existing infrastructure. The driver linac consist of three straight segments, LS1, LS2, LS3 and two folding segments FS1 and FS2.

DRIVER LINAC

Due to CW mode of the FRIB driver linac, the final beam power of 400 kW can be achieved with a low beam current which is below 1 emA for all ion species. The space charge effects are mostly negligible over the entire linac except in the ion source and low energy beam transport (LEBT). FRIB linac will be equipped with the state-of-the art high intensity superconducting ECR ion source capable to produce required intensity of heaviest ions in a single charge state. However, to operate the SC ECR with a large margin the linac was designed to accelerate two charge states of heaviest ions (e.g. U^{33+} and U^{34+}) up to the stripper [2]. To meet power requirement, a multiple charge state acceleration for the most ions heavier than argon is foreseen after the stripping at ~17 MeV/u [3].

In the FRIB design stage we have evaluated beam dynamics of the most critical beam of uranium with high statistics simulations in realistic conditions with all types of

---

errors and misalignments using the IMPACT [4] and TRACK [5] codes on high performance computers.

End-to-end Particle Tracking

The end-to-end simulation started with "realistic" distribution restored from emittance measurements of uranium beam extracted from the VENUS ion source [6]. The "realistic" distribution of two-charge-state uranium is then tracked through the Front End, LS1 and then five charge states (from U^{76+} through U^{80+}) were selected after the lithium stripper followed by another two acceleration segments [3]. The final beam phase space distributions at the fragmentation target are shown in Fig. 2. Beam-on-target requirements are met even for the most challenging multi-charge state uranium beam (e.g. >96 % of particles are within 1 mm diameter of beam spot size, all particles are within angular spread of ±5 mrad).
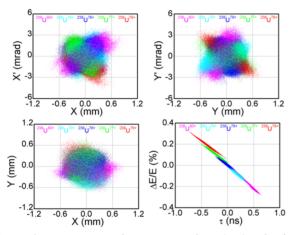

Figure 2: Transverse phase space plots (top), physical beam size (bottom-left), and longitudinal phase space (bottom-right) distributions on the target for 5-charge-state uranium without machine errors. Different colours represent 5 charge states of uranium.

Beam simulation studies with machine errors were performed to evaluate the linac performance under more realistic conditions [3]. When the element displacements are introduced, especially the misalignment of superconducting solenoids within ±1 mm, correctors must be set properly for the beam steering using BPMs' readings otherwise beam cannot be threaded through the linac. A total of 200 random seeds combining the errors were used in the multi-charge-state uranium beam simulations. In each seed run, one million particles were tracked from the exit of RFQ through the three linac segments to the fragmentation target. Figure 3 illustrates the maximum beam envelope (blue) at each longitudinal location of the 200 seeds together with the beam envelope without errors (green) and linac radial apertures (red). Beam evaluation results with machine errors show that the beam envelopes are well within apertures. Beam envelope growth is mainly due to misalignment (correctors were on) of the accelerator components. RF errors cause significant longitudinal emittance growth but it is not coupled into the transverse motion. No uncontrolled beam losses are observed with the nominal

errors. Although errors impact the beam distribution on target, beam-on-target requirements can be easily satisfied by final focusing quadrupoles and corrector magnets.
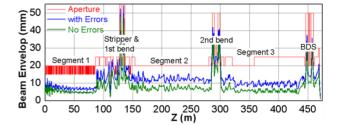

Figure 3: Beam envelopes along linac: beam element radial aperture in red, beam envelope without errors in green and with machine errors in blue.

Recent Beam Dynamics Studies

The average charge state of the ion beam after stripper strongly depends on the ions' atomic numbers. Therefore, after the stripper, contaminant ions will have different charge-to-mass ratios than the main beam. For example, for uranium, q/A=78/238=0.328 while for fully-stripped nitrogen q/A =0.5. The intensity of the contaminants can be as high as ~1% of the main beam power at the stripper which is ~40 kW for the FRIB 400 kW design power. The contaminant beam power impinging onto the charge stripper can be up to several hundred Watts and the loss of these contaminants must be controlled.

To avoid uncontrolled losses, we have designed a set of collimators installed along the FS1 that can intercept contaminant ions at relatively low energy of ~17 to 20 MeV/u depending on the ion species and localize losses in the designated areas with appropriate shielding as described in our recent publication [7]. The set of 10 collimators and charge selection slits slightly reduce the acceptance of the FS1 to avoid any beam losses in the LS2 and LS3. Figure 4 shows horizontal and vertical phase planes at the entrance of the LS2. As can be seen, the design beam emittance without any errors and other imperfections is well inside the FS1 acceptance (dark grey area). The latter is smaller than LS2 acceptance (pale grey area). Figure 4 shows the emittance and acceptance calculated for $^{238}U^{78+}$. Each uranium charge state has slightly different orientation of the beam phase space portraits and acceptances.
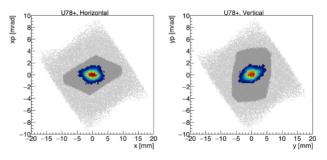

Figure 4: Transverse acceptance of the LS2 (pale grey), acceptance of the FS1 formed with all collimators (dark grey) and the design beam emittance at the entrance of the LS2.

HIGH-LEVEL PHYSICS CONTROLS SOFTWARE

The high-level physics controls software is under active development for FRIB accelerator system and it is mainly Python-based software ecosystem known as **P**hysics **H**igh-level **A**pplications a**n**d **T**oolkit for **A**ccelerator **Sy**stem, PHANTASY. It features the systematic solution to perform high-level physics controls in an efficient way and includes the following main components:

- The whole accelerator is represented as a hierarchical data structure. All the optics devices are modelled with unified software application programming interfaces (APIs), such that the user can talk to the devices in an object-oriented programming (OOP) way, rather than to the distributed power supply controls variables. PHANTASY provides Python classes to make this procedure standard and easy to do, the user can abstract FRIB accelerator (which is defined by the parameter named 'machine') with different segments ('segment'), e.g. LEBT, MEBT, etc. All the description of the accelerator is maintained by another package, which is updated once the machine configuration is changed.

- Interactive scripting environment for high-level physics controls. Once the accelerator is abstracted to OOP level, the users can implement the tuning algorithms to achieve various goals.

- Virtual accelerators solution. This is truly the same accelerator as the real FRIB accelerator from the view of EPICS controls; all the devices are named the same as FRIB accelerator. Powered by the so-called model engine, i.e. code to simulate the accelerator behaviour, the virtual accelerator supports testing of tuning algorithms.

- Interface to the different model engines. For instance, FLAME [8], IMPACT, TRACK etc, are developed or under development.

- Interface to different web services. For instance, 'channelfinder', which is a controls variables directory service, 'unicorn', which is home developed REST web service for unit conversion between physics and engineering fields.

- GUI applications. Finally, tuning algorithms are developed into a GUI application with PyQt5 [9], then all the users, including operators, can reach these automatically deployed apps from any workstation in the control room.

Example of Two-Charge State Beam Tuning

Due to the different synchronous phases for each charge state, the bunch centers in the phase space oscillate with respect to each other and result to effective emittance growth, as shown in Fig. 5. The two-charge-state ion beam should be tuned to overlap phase space images at the stripper location both in the transverse and longitudinal phase planes to minimize the emittance growth due to scattering and energy straggling as shown in Fig. 5.
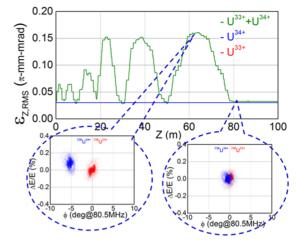

Figure 5: Longitudinal emittance of two-charge-state uranium beam along Segment 1 together with sampled particles (33+ red, 34+ blue) in longitudinal phase space.

Beam Central Trajectory Correction

Central trajectory correction could be achieved either by global parameter optimization or applying Orbit-Response-Matrix (ORM). The latter is being widely used on light sources like synchrotron and free-electron laser facilities. At FRIB, the ORM based central trajectory correction application is originally developed against virtual accelerator. The response matrix could be measured by altering the selected correctors one by one, and meanwhile, keep the BPM or wire-scanner readings for the beam central positions. The polynomial fitting can give the correspondent term of each corrector, in both horizontal and vertical direction. Then, with the trajectory to correct, the corrector settings could be calculated based on the inverse matrix of the measured ORM, usually, a singular-value decomposition (SVD) algorithm is applied to robustly figure out the inverse matrix. All these operations are being done in a user-friendly way, from the seamlessly integrated high-level physics applications.

Commissioning of Front End and First Three Cryomodules

A set of on-line physics applications have been developed for the setting of LEBT; optimal tuning of the Multi-Harmonic Buncher (MHB); beam central trajectory correction in LEBT, MEBT and cryomodules; quadrupole or solenoid scan for profile measurements and evaluation of rms emittance; longitudinal emittance rms evaluation by rotating beam image in the longitudinal phase space and measuring bunch length. Using these applications we were able to accelerate and characterize 33 μA argon beam up to 2.3 MeV/u through the first 3 cryomodules without notable beam losses as shown in Fig. 6. The signals from 15 BPMs along the MEBT, 3 cryomodules and diagnostics station are shown in Fig. 7. The results of quadrupole scan and beam rms size from the downstream profile monitor are shown in Fig. 8. Similar data measured with a silicon detector for the evaluation of the longitudinal emittance are shown in Fig. 9.
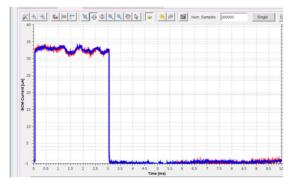
Figure 6: Beam peak current upstream (red) and downstream (blue) of the first three crymodules. Pulse length is 3 ms at 100 Hz repetition rate.

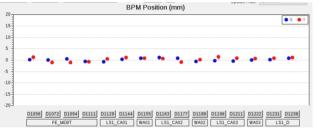

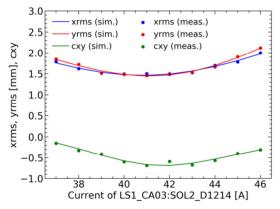Figure 7: BPM readings. Beam center deviation is within ±1.5 mm.

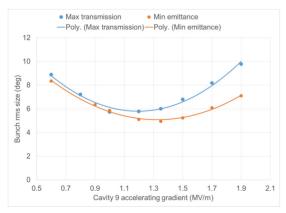Figure 8: Beam rms sizes and XY coupling term as a function of the quadrupole current in MEBT.

Figure 9: Beam longitudinal rms size as a function of the cavity accelerating gradient for two cases of the MHB tuning: (1) maximum transmission (blue) and (2) minimum longitudinal emittance (red).

ECR ION SOURCE SIMULATIONS

Due to complexity of physical processes, there is no fully self-consistent model of ECR ion sources (ECRIS). The existing computer models of ECRIS are based on various simplifications and use some empirical parameters to reproduce experimental data. The most comprehensive review of the current status of ECRIS simulations is given in [10].

We have decided to build a CST Particle Studio [11] model for the room temperature ECRIS in order to include two major factors strongly effecting the beam dynamics such as magnetization and space charge effects in the multi-component ion beam extracted from the ECRIS. The model includes 3D fields of the ion source but does not include plasma processes and stripping of ions. The simulation starts by generating a distribution of various ion charge states inside the resonance region of the ECR plasma. Then, the ions are tracked to the location of the extraction aperture. The analysis of ions distribution in the extraction aperture shows that rms beam parameters in the LEBT are mostly defined by the geometry of the extraction system and does not strongly depend upon the method how the ions are generated inside the plasma. Multiple ion charge states and ion species are extracted from the ECR assuming a flat plasma meniscus. The further tracking is performed in the presence of beam space charge and an external solenoidal field. These simulations show that a hollow beam structure in the real space (see Fig. 10) is formed due to the different focal length of the solenoid focusing for different ions and the presence of space charge. In addition, due to the large beam size in the solenoid, there is an effect of spherical aberrations.

The ion beam in the ECRIS is magnetized as a consequence there is a strong correlation term in the x-y′ and y-x′ phase planes after the beam extraction as shown in Fig. 11. We have also applied TRACK code for the 4D beam dynamics simulations of multi-component, multi-charge ion beam in the LEBT. Figure 12 shows the measured beam images along the LEBT together with simulated beam images in the same locations. Overall, the TRACK code reproduces the particle distribution in the real space.

So far, beam intensity in the LEBT was low, ~50 eμA. We expect to face more complicated beam dynamics issues when the beam current of a single ion specie will be higher by an order of magnitude. More advanced ECRIS models would be necessary to optimize ECRIS operational mode and beam transport with low emittance growth.
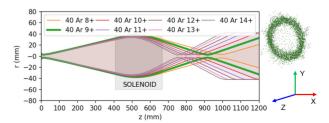

Figure 10: Envelopes of several charge states of argon after the extraction from ECRIS (left) and Ar⁹⁺ beam cross section in the focal plane of the solenoid (right).
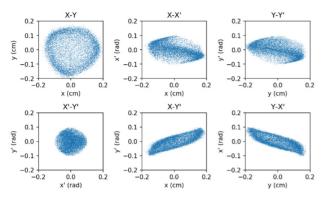
Figure 11: Simulated phase space plots in the Cartesian coordinates at the solenoid focal plane for $^{40}Ar^{9+}$.
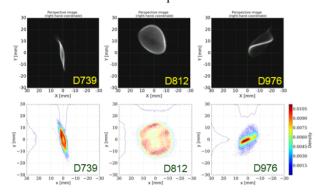

Figure 12: Measured (top) and simulated (bottom) beam images along the LEBT for $^{40}Ar^{9+}$.

BAYESIAN STATISTICS FOR MACHINE TUNING

We also aim on using statistical methods to gain information from the measured data. Below is an example of the application of Bayesian inference of the profile measurement to infer the unknown linearized beam distribution at the exit of the ECR source. The measurement data used in the inference is recorded using a beam viewer, located downstream of the first three electrostatic quadrupoles in the LEBT. The transverse beam size and the correlations vector $\sigma_i = (\sigma_x, \sigma_y, \sigma_{xy})$ in i^{th} measurement with the voltage setting $V_i = (V_i^1, V_i^2, V_i^3)$ is available. The linearized 4D distribution is to be inferred as 10 parameters: $\theta = (\epsilon_x, \beta_x, \alpha_x, \epsilon_y, \beta_y, \alpha_y, c_{xy}, c_{xy'}, c_{x'y}, c_{x'y'})$. We can use FLAME model to predict the measurement as $\sigma_{model,i} = f(V_i, \theta)$ and assume that the measurement only differs from the prediction by a Gaussian random number ξ_i with an amplitude $\delta = (\delta_x, \delta_y, \delta_{xy})$, which reads:

$$\sigma_{measure,i} = \sigma_{model,i} + \delta\xi_i.$$

Using the Bayesian formula as:

$$P(\theta, \delta \mid (\sigma_1, V_1), \ldots, (\sigma_i, V_i), \ldots)$$

$$= \frac{P((\sigma_1, V_1), \ldots, (\sigma_i, V_i), \ldots \mid \theta, \delta) P(\theta, \delta)}{P((\sigma_1, V_1), \ldots, (\sigma_i, V_i), \ldots)}$$

Since we assume the difference of the measurement and the model is Gaussian, the likelihood is written as

$$P((\sigma_1, V_1), \ldots, (\sigma_i, V_i), \ldots \mid \theta, \delta)$$

$$\sim \prod_i \frac{1}{\delta_x \delta_y \delta_{xy}} e^{-\frac{(\sigma_{measure,i} - \sigma_{model,i})^2}{2\delta^2}}$$

We can use Markov Chain Monte Carlo (MCMC) method to conduct the Bayesian inference [12] and reach saturation as shown in Fig. 13 for one of the parameters, the horizontal emittance. When the iteration reaches saturation, the result fit well with the experimental data. A similar behaviour is observed for all other 9 parameters of the beam distribution. In addition, we observed that the result of Bayesian inference fits better than the optimizer results, when comparing the fitting of the transverse correlation with standard beam optics methods.

We plan to continue using Bayesian method for machine tuning and expect that it will provide statistics information on reliability of beam parameters deduced from the measurements, better scaling to high dimensional problem, less local minimum problem and suggest the future experiments.
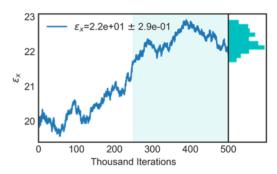

Figure 13: The saturation of the inference after 500K iteration of MCMC.

RARE ISOTOPE BEAMS

The layout of the FRIB target and fragment separators is shown in Fig. 14. Two software packages, COSY INFINITY [13] and LISE^{++} [14] have been heavily used for the design and optimization of the primary beam interaction with the target and transport of rare isotope beams. Due to the large beam emittance after the target, large aperture magnets and large momentum acceptance of the fragment separators, the 5th order optics in COSY INFINITY package has been applied for the design of fragment separators. The design has been verified with extensive Monte Carlo simulations using LISE^{++} code with embedded COSY IFINITY transport maps [15]. The simulations show that separation of isotopes on the selection slits is very small, a few mm. During the initial set-up of the fragment separators very large-scale simulations would be necessary to identify a specific isotope of interest among many unwanted products. The isotope of interest can be at very low intensity therefore parallel version of COSY and significant improvement of the LISE^{++} [14,16] are necessary for quick tuning of the transport and selection of isotopes for the experiments. This is especially important due to FRIB being a single user facility.

Figure 14: Layout of the beam FRIB experimental systems.

Preparation of Rare Isotopes for Post Acceleration

There are many nuclear physics experiments that require selection of particular isotopes and re-acceleration to ~3-12 MeV/u. Figure 15 shows current layout of the selection of isotopes in the fragment separator, stoppage in the helium gas cell, bunching in the RFQ cooler-buncher (RFQ CB) and charge breeding in the Electron Beam Ion Trap (EBIT), extraction from EBIT and injection to the post accelerator at 12 keV/u. The intensities of rare isotope beams produced by FRIB will be 4-5 orders of magnitude higher than currently available from the NSCL cyclotron. While there are several codes available for study and optimized design of the helium gas cell, RFQ CB and EBIT, there is no computer model that fully represents all processes in these devices such as 3D electromagnetic fields, interaction with gas atoms, charge-exchange reactions and most importantly space charge of ions. The space charge effects become crucial for the optimal design and operation of these devices with high intensity of isotope beams from FRIB. Therefore, development of such codes is critical for the FRIB science program.
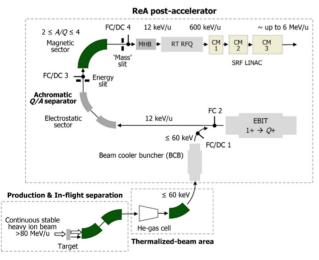

Figure 15: Preparation of secondary beams for injection into the post-accelerator.

CONCLUSION

Several well-established optimization and simulation codes were available for the design of FRIB accelerator and experimental systems. All these codes are being used for refining FRIB systems and transition to operation. Currently we are focused on the development of on-line physics applications for tuning of the driver linac and update of

the virtual accelerator model. The latter is being performed primarily to include the 3D maps of various electromagnetic devices and misalignment data of the accelerator components.

New parallel codes for large scale Monte Carlo simulation would be necessary for the quick setup of fragment separators and experiments with rare isotope beams. The intensities of rare isotope beams will be 4-5 orders of magnitude higher than in it is available now. Therefore, computer models of the devices for preparation of stopped rare isotope beams for post-acceleration should be updated to include 3D electromagnetic fields, interaction with gas atoms, charge-exchange reactions and, most importantly, space charge forces.

REFERENCES

[1] J. Wei *et al.*, "The FRIB Superconducting Linac - Status and Plans", in *Proc. LINAC'16*, East Lansing, MI, USA, Sep 2016. doi:10.18429/JACoW-LINAC2016-MO1A01

[2] E. Pozdeyev *et al.*, "FRIB Front End Design Status", in *Proc. LINAC'12*, Tel-Aviv, Israel, Sep 2012. http://jacow.org/LINAC2012/papers/thpb097.pdf

[3] Q. Zhao *et al.*, "FRIB Accelerator Beam Dynamics Design and Challenges", in *Proc. HB'12*, Beijing, China, Sep 2012, http://jacow.org/HB2012/papers/weo3b01.pdf

[4] J. Qiang *et al.*, *J. Comput. Phys.*, vol. 163, pp. 434, 2000.

[5] P. N. Ostroumov and K.W. Shepard, *Phys. Rev. ST. Accel. Beams,* vol. 11, pp- 030101, 2001.

[6] G. Machicoane *et al.*, "Design Status of ECR Ion Sources and LEBT for FRIB", in *Proc. ECRIS'12*, Beijing, China, Sep 2012. http://jacow.org/ECRIS2012/papers/thyo03.pdf

[7] P.N. Ostroumov *et al.*, "Accelerator Physics Advances in FRIB (Facility for Rare Isotope Beams)", in *Proc. IPAC'18*, doi:10.18429/JACoW-IPAC2018-THYGBF4

[8] Z. He *et al.*, *Phys. Rev. ST Accel. Beams,* vol 17, pp. 034001, March 2014.

[9] https://pypi.org/project/PyQt5/

[10] V. Mironov, *ICFA Beam Dynamics Newsletter*, no. 73, pp. 65-73, ed. G. Machicoane and P. N. Ostroumov, http://icfa-bd.kek.jp/Newsletter73.pdf

[11] https://www.cst.com/

[12] W. K. Hastings, *Biometrika*, vol. 57, no. 1, Apr 1970, pp. 97–109, doi:10.1093/biomet/57.1.97

[13] K. Makino and M. Berz, *NIM* A, vol. 585, pp. 346-350, 2006. http://bt.pa.msu.edu/index_cosy.htm

[14] O.B. Tarasov and D. Bazin, *NIM* B, vol. 376, pp. 185, 2016, http://lise.nscl.msu.edu

[15] M. Portillo and M. Hausmann, "Simulation of Rare Isotope Beam Production, Separation, and Delivery", FRIB internal report, FRIB-T40301-TD-000822-R001, 2015.

[16] M.P. Kuchera *et al.*, *NIM* B, vol. 376, pp. 168, 2016.

[17] A. Lapierre *et al.*, *Phys. Rev. Accel. Beams*, vol. 21, pp. 053401, 2018.